

Experimental investigation of the flow-induced vibration of a curved cylinder in convex and concave configurations

Gustavo R. S. Assi^{a,*}, Narakorn Srinil^b, Cesar M. Freire^c, Ivan Korkischko^{c,**}

^a*Department of Naval Architecture and Ocean Engineering, University of São Paulo, São Paulo, Brazil*

^b*Department of Naval Architecture and Marine Engineering, University of Strathclyde, Glasgow, UK*

^c*Department of Mechanical Engineering, University of São Paulo, São Paulo, Brazil*

Abstract

Experiments have been conducted to investigate the two-degree-of-freedom vortex-induced vibration (VIV) response of a rigid section of a curved circular cylinder with low mass-damping ratio. Two curved configurations, a concave and a convex, were tested regarding the direction of the flow, in addition to a straight cylinder that served as reference. Amplitude and frequency responses are presented versus reduced velocity for a Reynolds number range between 750 and 15,000. Results for the curved cylinders with concave and convex configurations revealed significantly lower vibration amplitudes when compared to the typical VIV response of a straight cylinder. However, the concave cylinder showed relatively higher amplitudes than the convex cylinder which were sustained beyond the typical synchronisation region. We believe this distinct behaviour between the convex and the concave configurations is related to the wake interference taking place in the lower half of the curvature due to perturbations generated in the horizontal section when it is positioned upstream. Particle-image velocimetry (PIV) measurements of the separated flow along the cylinder highlight the effect of curvature on vortex formation and excitation revealing a complex fluid-structure interaction mechanism.

*Corresponding author: g.assi@usp.br. Address: PNV Dept. Eng. Naval e Oceânica, Escola Politécnica da Universidade de São Paulo, Av. Prof Mello Moraes 2231, 05508-030, São Paulo - SP, Brazil. www.ndf.poli.usp.br.

**Now at the Institute of Aerodynamics and Flow Technology, German Aerospace Center (DLR), Göttingen, Germany.

Keywords:

Vortex-induced vibration, Cross-flow and in-line motion, Curved cylinder,
Particle image velocimetry

Nomenclature

D Cylinder external diameter
 h Cylinder vertical length below the water line
 m^* Mass ratio
 ζ Structural damping ratio
 f_0 Natural frequency in air
 U Flow speed
 U/Df_0 Reduced velocity
 \hat{x} Streamwise harmonic amplitude of vibration
 \hat{y} Cross-flow harmonic amplitude of vibration
 f_x Streamwise oscillation frequency
 f_y Cross-flow oscillation frequency
Re Reynolds number

1. Introduction

2 Ongoing deep-sea exploration, installation and production of hydrocar-
3 bon energy need the development of new viable technologies. One of these
4 is the requirement of a robust and reliable analysis tool for the prediction of
5 vortex-induced vibration (VIV) of marine structures exposed to ocean cur-
6 rents. Because VIV can cause high cyclic-loading fatigue damage of struc-
7 tures, it is now widely accepted to be a crucial factor that should be taken
8 into account in the preliminary analysis and design. However, many in-
9 sightful VIV aspects are still unknown and far from fully understood; these
10 render the structural design quite conservative with the use of a large factor
11 of safety. For offshore structures with initial curvatures and high flexibil-
12 ity such as catenary risers, mooring cables and free-spanning pipelines, the
13 theoretical, numerical or experimental VIV research is still very lacking.

14 Risers are very long pipes used to carry oil from the sea bed to offshore
15 platforms floating on the water surface. Under the effect of sea currents,
16 these flexible structures are especially susceptible to flow-induced vibrations,
17 particularly since they have a relatively low mass compared to the mass of
18 the displaced fluid. Generally, an offshore floating platform accommodates
19 several riser pipes together with many other cylindrical structures. The

20 interaction of these flexible structures can produce an even more complex
21 problem, resulting in vibrations with rather unexpectedly higher amplitudes
22 (Assi et al., 2010). Flow interference from the platform hull, the soil on
23 sea bed and the pipe itself can also increase the complexity of the flow,
24 generating complex responses.

25 The riser may respond with different amplitudes and frequencies de-
26 pending on the flow excitation and structural stiffness along the length of
27 the pipe. Consequently, several modes of vibration with varying curvature
28 appear along the span resulting in a very rich fluid-structure interaction
29 mechanism (Srinil, 2010). In addition to that, flexible risers can be laid
30 out in a catenary configuration which results in high curvature close to the
31 region where it touches the bottom of the ocean, called the touchdown point.

32 In an attempt to understand and model the fluid-dynamic behaviour
33 around curved sections of risers we have performed experiments with a
34 curved, rigid circular cylinder in a water channel. This idealised experi-
35 ment is far from reproducing the real conditions encountered in the ocean;
36 nevertheless it should throw some light on understanding how the vortex
37 shedding mechanism is affected by the curvature of the pipe. In addition to
38 the phenomenological aspects, the present work may also serve as reference
39 for validation and benchmarking of numerical simulations of fluid-structure
40 interaction.

41 An investigation into the vortex shedding patterns and the fundamental
42 wake topology of the flow past a stationary curved circular cylinder has been
43 carried out by Miliou et al. (2007) based on computational fluid dynamics
44 studies. As a result of pipe initial curvatures, flow visualizations highlight
45 different kinds of wake characteristics depending on the pipe (convex or
46 concave) configuration and its orientation with respect to (aligned with or
47 normal to) the incoming flow. When the flow is uniform and normal to
48 the curvature plane, the cross-flow wake dynamics of curved pipes behave
49 qualitatively similar to those of straight pipes. This is in contrast to the
50 case of flow being aligned with the curvature plane where wake dynamics
51 change dramatically. However, these scenarios are pertinent to a particular
52 stationary cylinder case in a very low-Reynolds number range. The VIV
53 behaviour will further transform if the structure oscillates and interacts with
54 the fluid wakes, depending on several fluid-structure parameters.

55 **2. Experimental arrangement**

56 Experiments have been carried out in the Circulating Water Channel
57 of the NDF (Fluids and Dynamics Research Group) at the University of

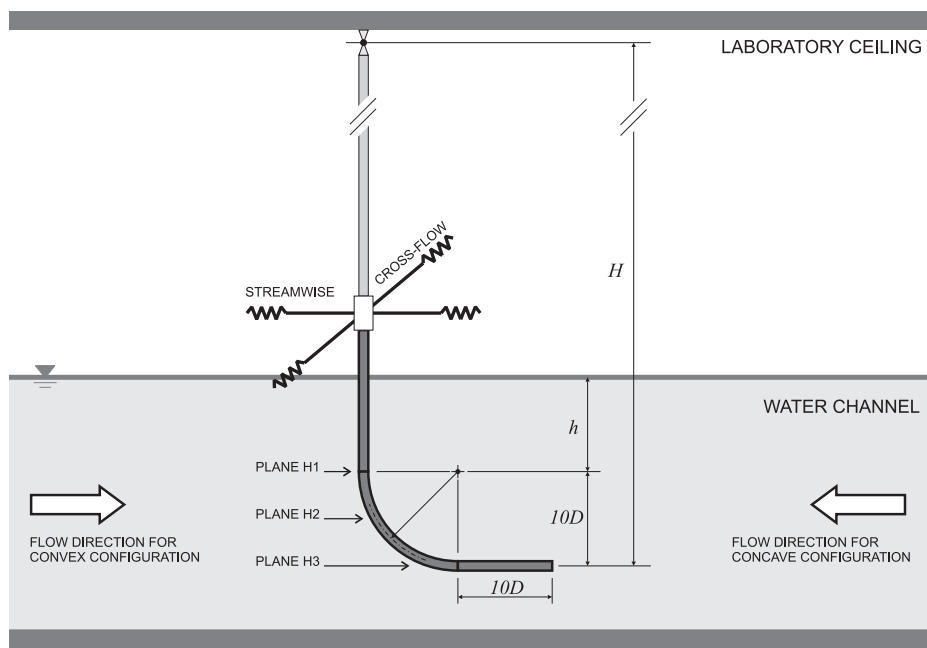


Figure 1: Experimental arrangement in the NDF-USP circulating water channel. The cylinder was rotated by 180 degrees to arrange concave and convex configurations.

58 São Paulo, Brazil. The NDF-USP water channel has an open test section
59 0.7m wide, 0.9m deep and 7.5m long. Good quality flow can be achieved
60 up to 1.0m/s with turbulence intensity less than 3%. This laboratory has
61 been especially designed for experiments in flow-induced vibrations and more
62 details about the facilities are described in Assi et al. (2006).

63 A rigid section of a curved circular cylinder, with an external diameter
64 of $D = 32\text{mm}$, was made of ABS plastic and Perspex tubes according to
65 the dimensions shown in Figure 1. The curved cylinder was composed of a
66 horizontal section with $10D$ in length, a curved section with a $10D$ radius
67 and a vertical section with length h/D that could be varied with reference
68 to the water line. The water level was set to 700mm from the floor of the
69 channel, which meant that the $10D$ -long horizontal part of the cylinder was
70 not close enough to the floor to suffer interference from the wall.

71 The model was connected by its upper end to a long pendulum rig (length
72 $H = 3.0\text{m}$) that allowed the system to oscillate in two degrees of freedom
73 (2dof) in the cross-flow and streamwise directions. The model was attached
74 to two pairs of coil springs that provided the stiffness of the system. The
75 springs were set to provide the same natural frequency (f_0 , measured in air)
76 in both the cross-flow and streamwise directions. The design and construction
77 of the pendular elastic rig was made by Freire & Meneghini (2010) based
78 on a previous idea employed by Assi et al. (2009, 2010b) for experiments
79 with VIV suppressors. The present apparatus has been validated for VIV
80 experiments by Freire et al. (2009, 2011).

81 Two laser sensors measured the cross-flow and streamwise displacements
82 of the pendulum referring to the displacement of the bottom tip of the mod-
83 els. A load cell was installed before the springs to allow for instantaneous
84 measurements of lift and drag acting on the cylinder. (Hydrodynamic forces
85 will not be discussed in this paper.) A particle-image velocimetry (PIV)
86 system was employed to analyse the instantaneous wake patterns along the
87 cylinder span.

88 Regarding the flow direction, two orientations were investigated: a con-
89 vex and a concave configuration according to the direction of the flow ap-
90 proaching the curvature. The flow direction in the test section of the water
91 channel was not changed; naturally the curved cylinder was rotated by 180
92 degrees to allow for both concave and convex arrangements. This is also
93 illustrated in Figure 1.

94 Decay tests have been performed in air in order to determine the natural
95 frequencies of the system in both directions as well as the level of structural
96 damping. The apparatus with one universal joint and four springs turned
97 out to present a very low structural damping of $\zeta = 0.2\%$, measured as a

Table 1: Structural properties.

	m^*	ζ	$m^*\zeta$
Straight cylinder	2.8	0.2%	0.0056
Curved cylinders	2.1	0.2%	0.0042

98 fraction of the critical damping. The total oscillating mass of the system was
 99 measured in air, resulting in a non-dimensional mass ratio m^* , defined as the
 100 ratio between the total mass and the mass of displaced fluid. Consequently,
 101 the mass-damping parameter $m^*\zeta$ of the system was kept to the lowest
 102 possible value in order to amplify the amplitude of response.

103 Table 1 presents a summary of the structural parameter for both the
 104 straight and curved cylinder.

105 3. Results for a straight cylinder

106 A preliminary VIV experiment was performed with a straight cylinder
 107 in order to validate the set-up and generate data for comparison. The same
 108 pendulum rig was employed, only replacing the curved model by a straight
 109 cylinder with the same diameter. This time, the straight cylinder was long
 110 enough to reach the bottom wall only leaving a 3mm clearance to allow for
 111 free movement of the pendulum in any direction.

112 The dynamic response of the straight cylinder covered a reduced velocity
 113 range from 1.5 to 12, where reduced velocity (U/Df_0) is defined using the
 114 cylinder natural frequency of oscillation measured in air. The only flow
 115 variable changed during the course of the experiments was the flow velocity
 116 U , which, as for full-scale risers, alters both the reduced velocity and the
 117 Reynolds number between 750 and 15,000 for a maximum reduced velocity
 118 of 20.

119 The flow around a smooth, straight circular cylinder in the considered
 120 Reynolds number range (identified as sub-critical) is generally expected to
 121 be three-dimensional, with a laminar boundary layer over the cylinder sur-
 122 face and turbulent vortex wake. However, in the case of curved cylinder,
 123 the curvature plays a significant role in modifying the wake dynamics, which
 124 depends on the leading geometry facing the approaching flow. This entails
 125 both the normal and axial flow components along the cylinder curved sec-
 126 tion, further complicating the spatio-temporal vortex shedding mechanisms,
 127 associated forces and frequencies. This has been exemplified by Miliou et
 128 al. (2007) for $Re = 500$.

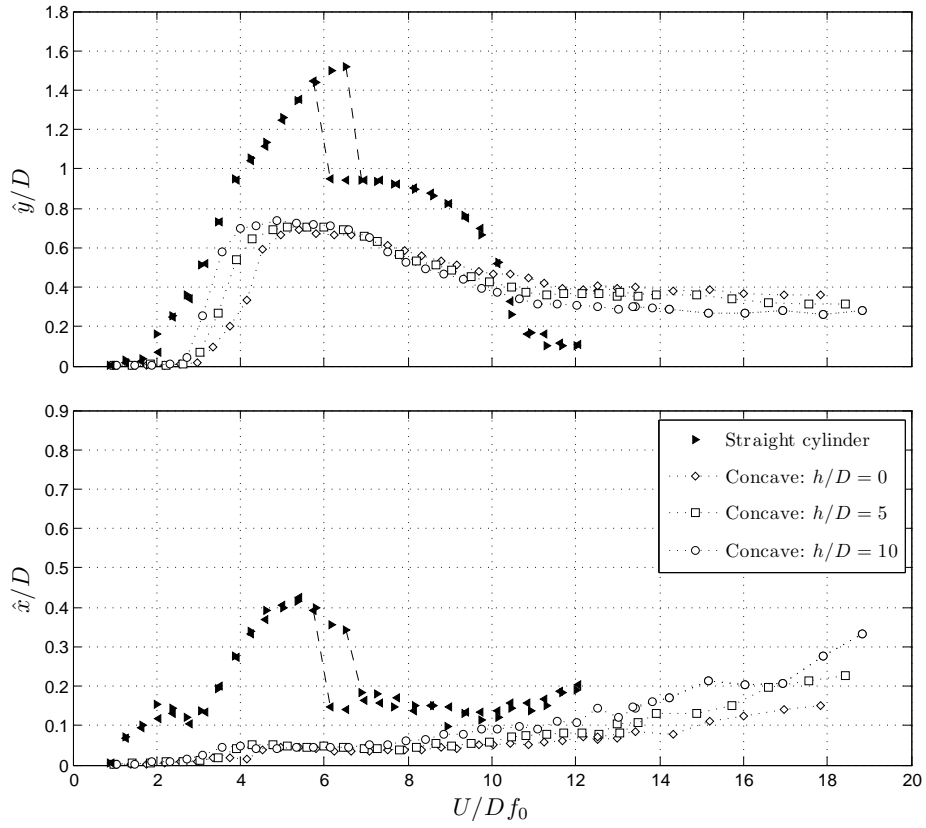


Figure 2: Cross-flow (\hat{y}/D) and streamwise (\hat{x}/D) amplitude of vibration versus reduced velocity for a straight cylinder and concave configurations varying the vertical section length (h/D). Symbols \blacktriangleright are for runs with increasing flow speed, while \blacktriangleleft are for decreasing.

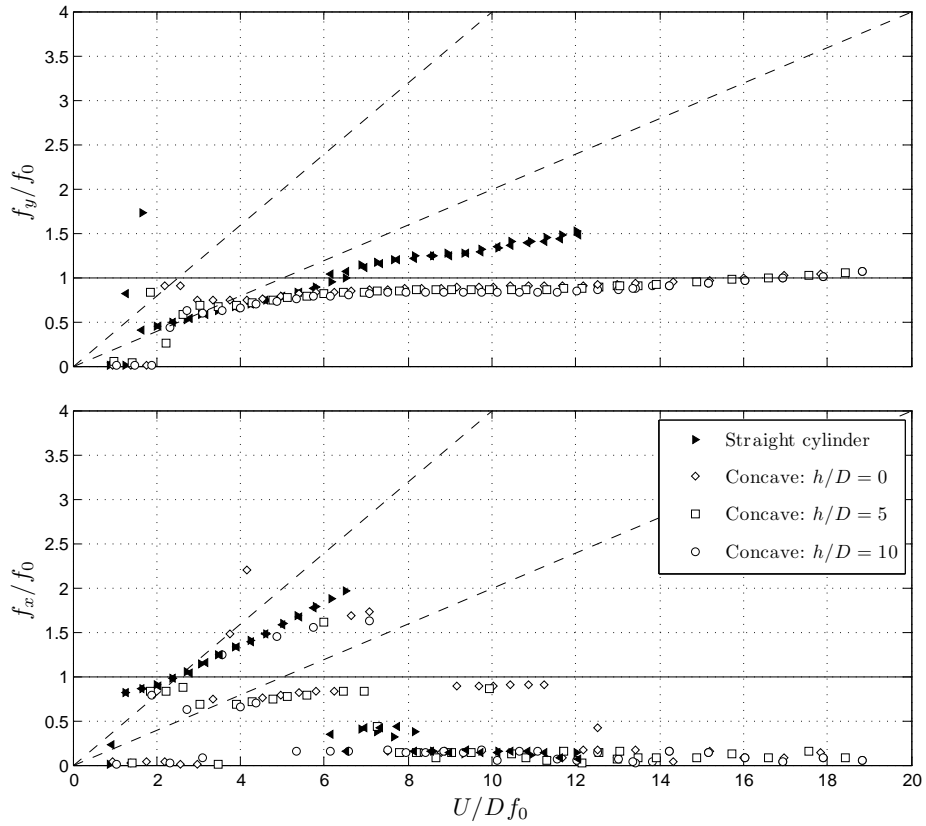


Figure 3: Cross-flow (\hat{y}/D) and streamwise (\hat{x}/D) dominant frequency of response versus reduced velocity for a straight cylinder and curved concave configurations varying the vertical section length (h/D). Symbols \blacktriangleright are for runs with increasing flow speed, while \blacktriangleleft are for decreasing.

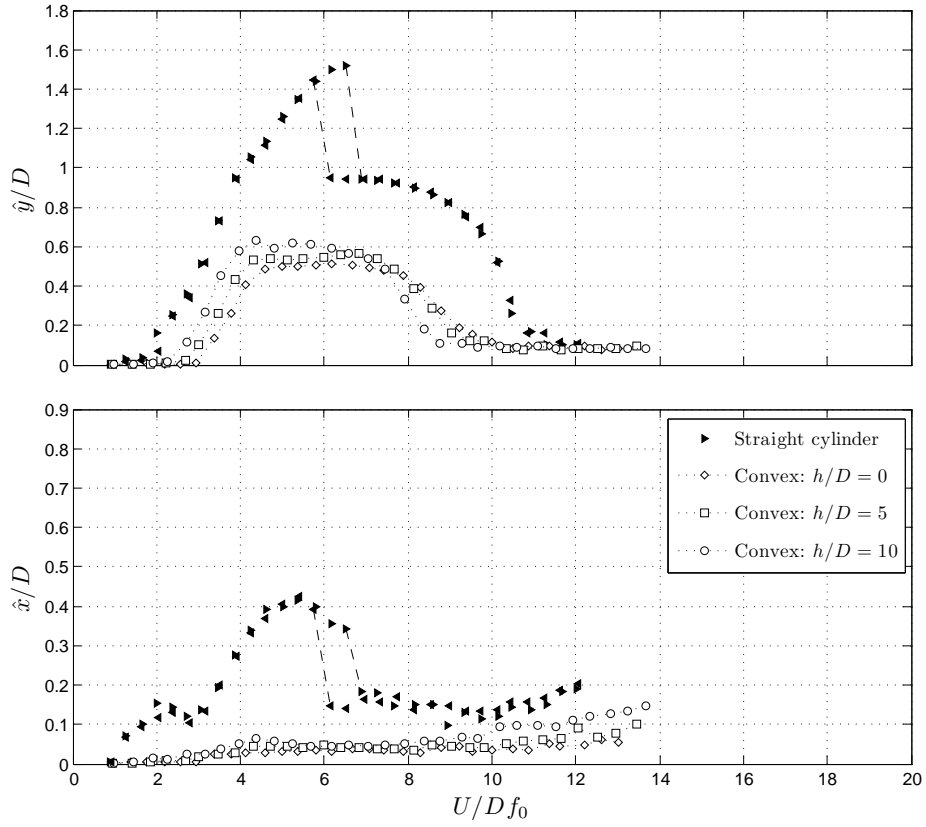


Figure 4: Cross-flow (\hat{y}/D) and streamwise (\hat{x}/D) amplitude of vibration versus reduced velocity for a straight cylinder and convex configurations varying the vertical section length (h/D). Symbols \blacktriangleright are for runs with increasing flow speed, while \blacktriangleleft are for decreasing.

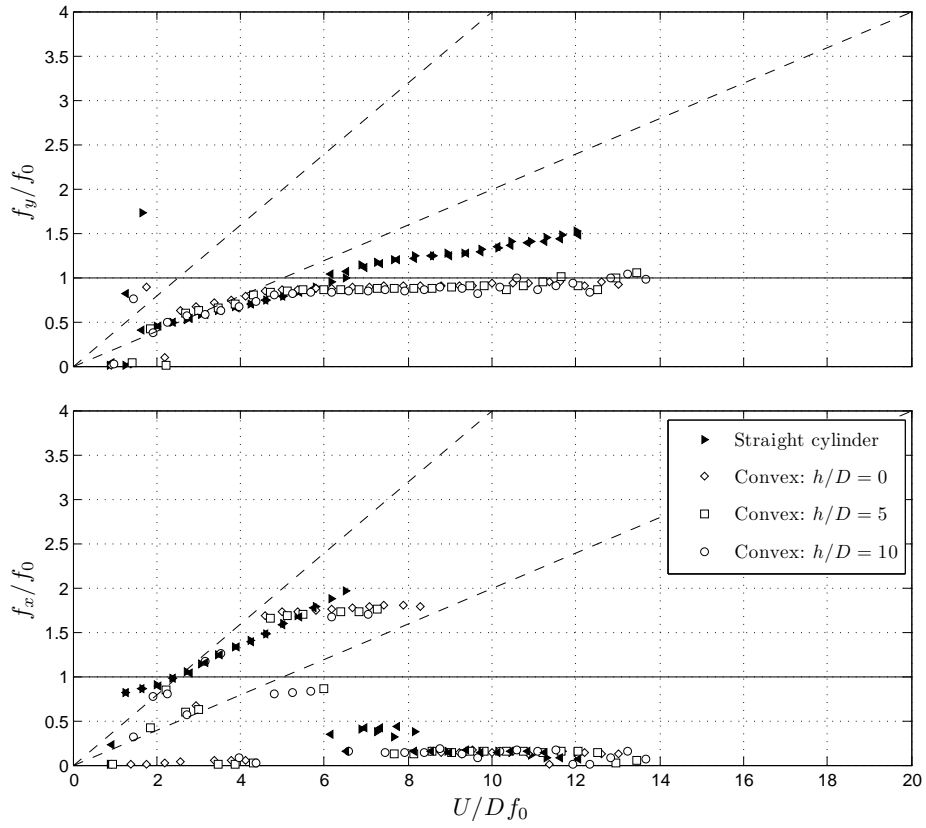


Figure 5: Cross-flow (\hat{y}/D) and streamwise (\hat{x}/D) dominant frequency of response versus reduced velocity for a straight cylinder and curved convex configurations varying the vertical section length (h/D). Symbols \blacktriangleright are for runs with increasing flow speed, while \blacktriangleleft are for decreasing.

129 Throughout the study, cylinder displacement amplitudes (\hat{x}/D for the
130 streamwise and \hat{y}/D for the cross-flow directions) were found by measuring
131 the root mean square value of response and multiplying by the square root
132 of 2 (the so called harmonic amplitude). This is likely to give an underes-
133 timation of maximum response but was judged to be perfectly acceptable
134 for assessing the general behaviour of VIV, since the response is mostly
135 harmonic. Results presented in the present study correspond to the dis-
136 placement of the lowest point of the model, i.e., the end of the cylinder
137 closer to the section floor, thus representing the maximum displacement de-
138 veloped by each model. Consequently, the equivalent amplitude at the water
139 surface for the cylinder with a $10D$ vertical section is 20% smaller than the
140 amplitude indicated in the results. Applying similar corrections, amplitudes
141 are 16% smaller for the cylinder with a $5D$ vertical section and 11% smaller
142 for the cylinder with no vertical section.

143 Displacements are non-dimensionalised by the cylinder diameter D . The
144 dataset for the straight cylinder is repeated in Figures 2 to 5 to serve as
145 reference.

146 Figures 2 and 4 compare the reference cross-flow and streamwise re-
147 sponses obtained from two different runs with the straight cylinder. In the
148 first one, the flow speed (U) was increased in 30 steps from zero to a maxi-
149 mum, while in the second it was decreased from the maximum to zero. Both
150 data sets overlap rather well for all the reduced velocity range except for a
151 region around $U/Df_0 = 6$ where the well-known phenomenon of hysteresis
152 in the VIV response has been observed. The streamwise VIV response also
153 seems to occur in two resonance ranges ($U/Df_0 = 2$ and 6), the so-called
154 second and third instability ranges involving asymmetric vortices (Bearman,
155 1984).

156 Although the observed peak amplitude of $\hat{y}/D = 1.5$ around $U/Df_0 = 6$
157 is slightly higher than other results found in the literature for similar values
158 of $m^*\zeta$ (for example, Assi et al., 2009) the general behaviour of both curves
159 show a typical response for 2-dof VIV. The higher amplitude found here
160 could be explained by the very low mass-damping characteristics of the
161 system and the geometric projection of the amplitude at the tip of the
162 model and not at mid-length as usual.

163 Although the cylinder was initially aligned in the vertical position, in
164 flowing water the mean drag displaces the cylinder from its original location
165 reaching a slightly inclined configuration from the vertical. This was judged
166 not to be detrimental to the experiment; hence the inclination of the cylinder
167 was not corrected between each step. The same procedure was adopted for
168 the curved cylinder.

169 Figures 3 and 5 present the dominant frequency of response versus re-
 170 duced velocity. Two dashed lines inclined with different slopes represent the
 171 region for a Strouhal number of 0.2 and 0.4, i.e., an estimation of the vortex
 172 shedding frequency for a straight cylinder in the cross-flow and streamwise
 173 direction respectively. It is clear that the straight cylinder presents a typical
 174 VIV response oscillating in the cross-flow direction with a frequency follow-
 175 ing the $St = 0.2$ line up to the beginning of the upper branch. Eventually,
 176 f_y/f_0 departs from $St = 0.2$ towards the unity value around $U/Df_0 = 6$.
 177 The behaviour observed for the streamwise vibration is also typical of VIV
 178 with the difference that the frequency of response is twice as that for the
 179 cross-flow direction during much of the synchronisation range.

180 4. Response of the curved cylinder

181 As mentioned above, experiments with the curved cylinder were per-
 182 formed taking into account two distinct configurations as far as the flow
 183 direction is concerned. In the concave configuration the flow approaches the
 184 model reaching first the horizontal section. As opposed to that, in the con-
 185 vex configuration the horizontal section is placed downstream of the curved
 186 and vertical parts.

187 4.1. Amplitude of vibration

188 In general terms, as presented in Figures 2 and 4, the curved cylinders
 189 showed significantly less vibration for both concave and convex configura-
 190 tions when compared to the typical VIV response of the straight cylinder.
 191 Such a reduction is noticeable in both the cross-flow and streamwise re-
 192 sponses. This clearly shows that the curvature of the cylinder modifies the
 193 vortex shedding mechanism in a manner that the structure extracts less en-
 194 ergy from the flow. We shall return to this point when investigating the
 195 velocity flow field with PIV.

196 For each concave and convex configuration, the vertical section of the
 197 cylinder close to the free surface was varied in three different lengths: $h/D =$
 198 0, 5 and 10. The overall response for the three values of h/D is very similar,
 199 showing only minor differences at the beginning of the synchronisation range
 200 between $U/Df_0 = 3.0$ and 5.0. Apart from that, no distinct behaviour was
 201 observed as far as a variation in h/D is concerned for both concave and
 202 convex configurations.

203 The cross-flow displacement does not reveal distinct upper and lower
 204 branches of vibration such as those observed for a straight cylinder, but it
 205 produces a smooth curve that spans the whole synchronisation region with

206 maximum amplitude around $\hat{y}/D = 0.75$ for the concave and 0.65 for the
207 convex configurations. No hysteresis is found.

208 However, the most interesting feature of such a behaviour is found when
209 the convex response is compared to the concave one (Figures 2 and 4). While
210 the convex curve for \hat{y}/D drops immediately between $U/Df_0 = 8$ and 10 to a
211 level of $\hat{y}/D \approx 0.1$, the response for the concave case does not diminish, but is
212 sustained for higher reduced velocities around $\hat{y}/D = 0.3$ until the end of the
213 experiment. Apparently there must be a fluid-elastic mechanism occurring
214 for reduced velocities above 8.0 for the concave configuration capable of
215 extracting energy from the flow to sustain vibrations around $\hat{y}/D = 0.3$.
216 We shall discuss this point later while analysing the PIV flow fields.

217 In the streamwise direction the responses of the curved cylinders are dif-
218 ferent from the typical VIV developed by the straight cylinder. Streamwise
219 vibrations in the first and second resonance regions are totally suppressed,
220 probably owing to the hydrodynamic damping effect induced by the cylin-
221 der's horizontal part. At the same time, the streamwise vibration \hat{x}/D for
222 the concave case also shows increasing amplitude beginning at reduced ve-
223 locities higher than 10 and reaching $\hat{x}/D \approx 0.35$ for the highest flow speed.
224 It coincides with the increased amplitude observed in the cross-flow direc-
225 tion and should be related to the same excitation mechanism. Once more,
226 no distinct difference in the streamwise response was observed while varying
227 h/D .

228 4.2. Frequency of vibration

229 Figures 3 and 5 present the dominant frequency of oscillation non-dimensionalised
230 by the natural frequency for both cross-flow and streamwise directions of
231 motion. Results for the curved cylinder show a consistent behaviour in the
232 cross-flow direction, with data points following the Strouhal line up to the
233 upper branch peak but remaining closer to $f_y/f_0 = 1.0$ for the rest of the
234 reduced velocity range. In the streamwise direction, we find data points fol-
235 lowing both Strouhal lines and also very low frequencies indicating random
236 drifts instead of periodic oscillations. Since the displacements in the stream-
237 wise direction are much smaller for the curved cylinder than the straight one,
238 we should expect broader frequency spectra dominating over the response.

239 One might remember that the straight and curved cylinder should have
240 very similar values of added mass in the cross-flow direction, but slightly
241 different values in the streamwise direction due to the geometric properties
242 relative to the flow. We have not taken such effect into account in this
243 paper, but it might be playing an important role defining the frequencies of
244 oscillation in water.

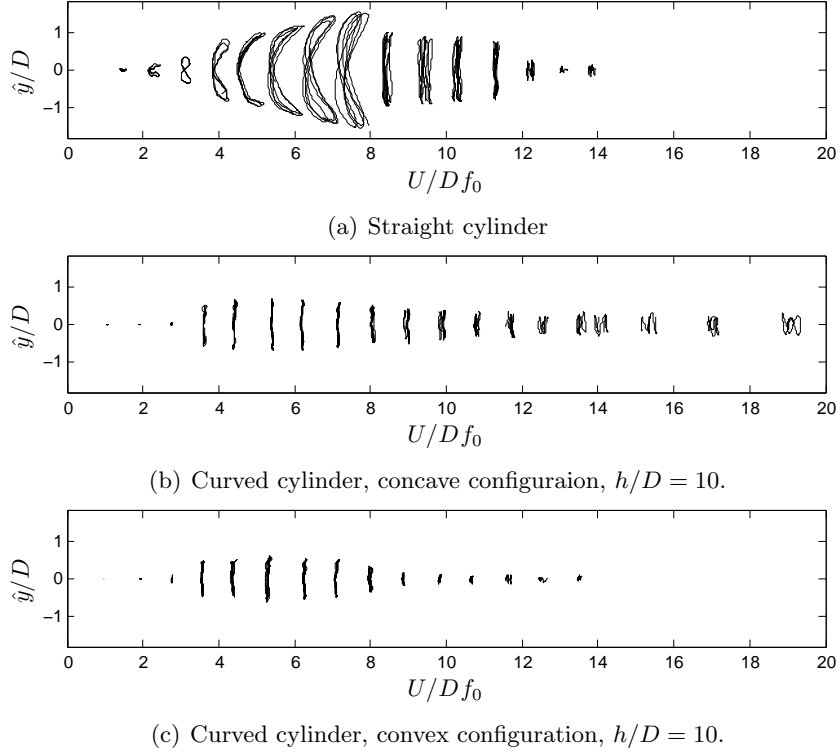


Figure 6: Response trajectories of motion for a (a) straight cylinder and a curved cylinder in (b) concave and (c) convex configurations. Each trajectory was taken at the reduced velocity indicated in the horizontal axis.

245 4.3. Trajectories of motion

246 Figure 6 qualitatively compares samples of displacement trajectories ob-
 247 tained for three experiments performed with the straight cylinder and the
 248 curved cylinders with $h/D = 10$. The straight cylinder presents distinct
 249 eight-shape figures typical of 2dof VIV owing to the 2:1 ratio on the stream-
 250 wise to cross-flow frequency of excitation. On the other hand, trajectories
 251 for both configurations of the curved cylinder reveal that the streamwise
 252 displacement is greatly reduced when compared to the straight cylinder.
 253 Both concave and convex cases show very little movement in the streamwise
 254 direction for the whole range of reduced velocity.

255 Another interesting observation relates to the movement of both curved
 256 cylinders. It is clear that for reduced velocities greater than 10 the convex
 257 cylinder shows small displacements in both directions, while vibrations are
 258 sustained until the end of the experiment for the concave case as shown in

259 Figures 2 and 4.

260 **5. Velocity and vorticity fields of stationary cylinders**

261 Two dimensional PIV (particle image velocimetry) measurements of the
262 flow around the cylinder were performed, for both concave and convex con-
263 figurations, on a vertical plane parallel to the plane of curvature. In addition,
264 PIV measurements were also performed on three horizontal planes (marked
265 H1, H2 and H3 in Figure 1 across the cylinder diameter.

266 All PIV measurements were taken for $Re = 1000$ in the sub-critical
267 Reynolds number regime found for a straight circular cylinder. According
268 to Williamson (1996), the particular flow is in the shear-layer transition
269 regime, characterised by an increase on the base suction, a gradual decrease
270 in the Strouhal number and a decrease in the formation length of the mean
271 recirculation region. These trends are caused by the developing instability
272 of the separating shear layers from the sides of the body. The flow around
273 a curved cylinder, which presents different elliptical cross-sections along the
274 span, may behave slightly different from the above description. Further
275 investigation is necessary in order to evaluate that.

276 *5.1. Vertical plane*

277 We shall start discussing the results obtained from the vertical plane, as
278 presented in Figures 7 to 12. Four visualisation areas for each configuration,
279 labelled A1 to A4, were conveniently distributed along the length of the
280 cylinder in order to evaluate as much as possible to the flow pattern around
281 the body. All four areas are in the same plane illuminated by the laser,
282 which is parallel to the plane of curvature only dislocated by $1D$ from the
283 centre of the cylinder towards the camera in order to capture the highest
284 velocities induced by the vortex tubes. Figures 9 and 12 show the location
285 of each area composing the flow field along the cylinder. It is important
286 to note that each velocity field was obtained from a different acquisition
287 instant; hence A1, A2, A3 and A4 are not correlated in time.

288 All PIV measurements were performed for a static cylinder at $Re \approx 1000$.
289 Of course the wake pattern for the static cylinder is expected to be different
290 from the wake of an oscillating cylinder, but even an analysis of a fixed
291 body can contribute to the understanding of the complex vortex-structure
292 interaction occurring during the response. A similar approach was employed
293 by Miliou et al. (2007) who performed numerical simulations for a static,
294 curved cylinder between $Re = 100$ and 500 . The same colour scales have

295 been employed from Figures 7 to 12 to allow for direct comparison of velocity
296 magnitude and vorticity contours.

297 With that in mind, let us analyse first the flow pattern around the concave
298 configuration in Figures 7 to 9. The overall flow around the body can
299 be divided in two parts:

300 (I) Areas A1 and A2 show the region where the flow is mostly parallel to
301 the axis of the cylinder. Therefore, no clear vortex tubes are observed with
302 concentrated axial vorticity. Instead, the flow along the horizontal length is
303 disturbed by the separation occurring at the tip of the cylinder. Area A1
304 shows the flow approaching the disk facing upstream and separating into a
305 recirculation bubble. The periodicity of the shedding associated with this
306 region is also related to the flow speed and the diameter D , but no coherent
307 vortices parallel to the cylinder are able to form. As a consequence, a cascade
308 of small vortices is convected downstream along the horizontal length (see
309 area A2) reaching the beginning of the curved section.

310 (II) Areas A3 and A4 show the region where the flow is mainly perpen-
311 dicular to the axis of the cylinder. Coherent vortex tubes tend to form fol-
312 lowing the curvature of the body, but further downstream they are stretched
313 and rapidly breakdown into smaller vortices that are convected by the flow.
314 Area A3 shows the instant when a vortex tube is shed almost tangent to
315 the curvature, while area A4, around the vertical section, reveal a formation
316 region more or less aligned with the axis of the cylinder. Streamlines drawn
317 in areas A3 and A4 reveal a non-negligible velocity component deflecting
318 the flow downwards immediately after the vortex formation region. As we
319 move along the cylinder towards the water line from A3 to A4 the down-
320 ward component is gradually reduced until it eventually disappears towards
321 the upper half of A4. This region marks the competition between two wake
322 modes existent along the transition from curved to straight cylinder. This
323 looks similar to Figure 15 in Miliou et al. (2007), with $Re = 100$, although
324 without the cylinder horizontal section therein.

325 Analysing the flow pattern for the convex configuration in Figures 10 to
326 12 we notice two striking differences:

327 Firstly, because the flow approaching the convex body does not encounter
328 a blunt disk facing upstream, no strong separation or recirculation bubble
329 is formed. As a consequence, the horizontal section seen in areas A1 and
330 A2 is not exposed to a disturbed, unsteady flow parallel to the axis of the
331 cylinder. In fact, A1 and A2 reveal that the upper half of the horizontal
332 length is exposed to a periodic flow formed by a regular wake, while the
333 bottom half experiences almost no perturbation, with streamlines showing
334 a well behaved flow field parallel to the axis.

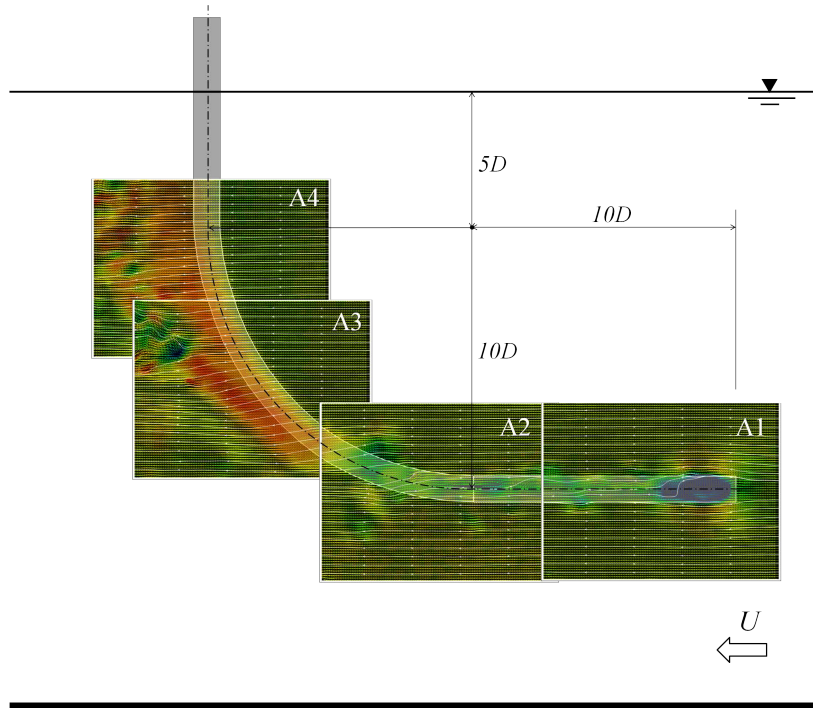


Figure 7: Composition of instantaneous PIV velocity fields for concave configuration with $h/D = 5$.

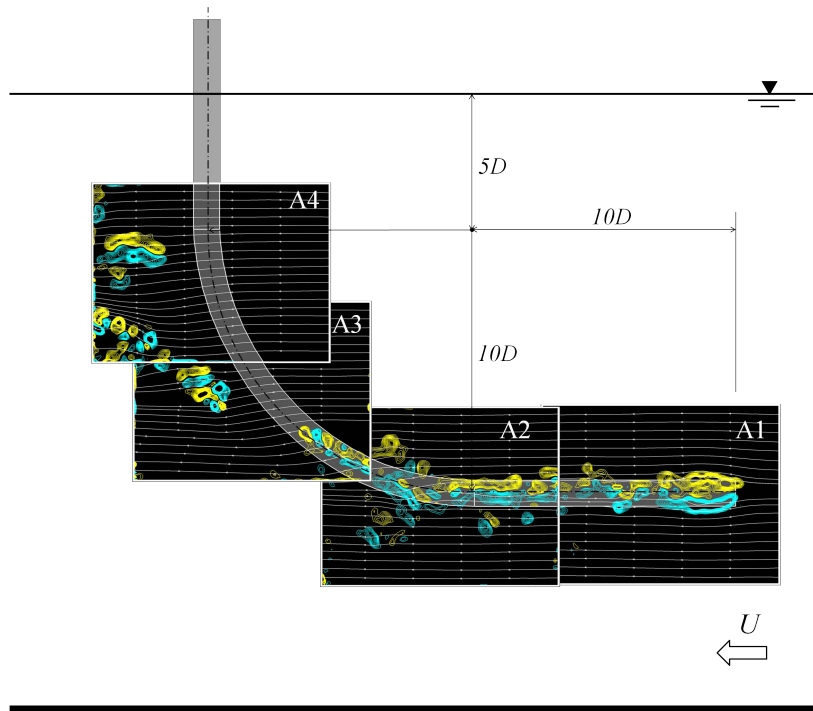


Figure 8: Composition of instantaneous PIV vorticity fields for concave configuration with $h/D = 5$.

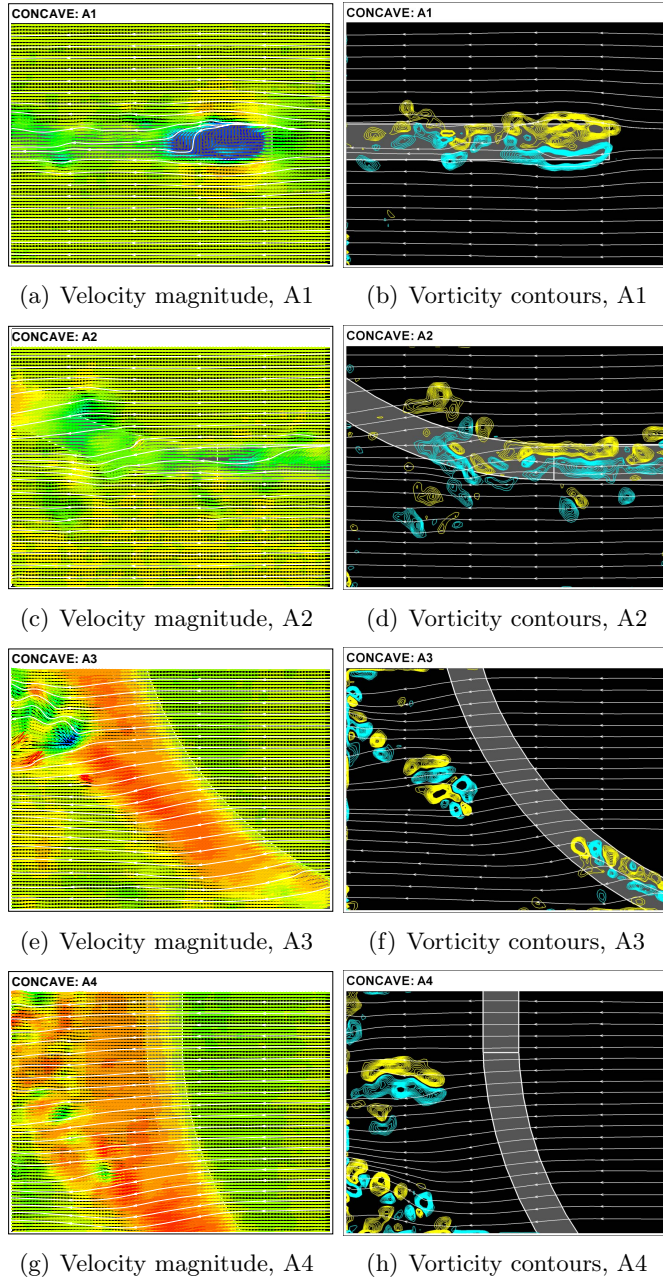


Figure 9: Detailed velocity and vorticity fields from Figures 7 and 8. Flow direction is from right to left. $Re = 1000$. Colour scale for velocity magnitude is from 0.004m/s (blue) to 0.05m/s (red). Colour scale for vorticity contours is in the range $\pm 0,004\text{s}^{-1}$. (Velocity fields do not correspond to the vorticity fields in time.)

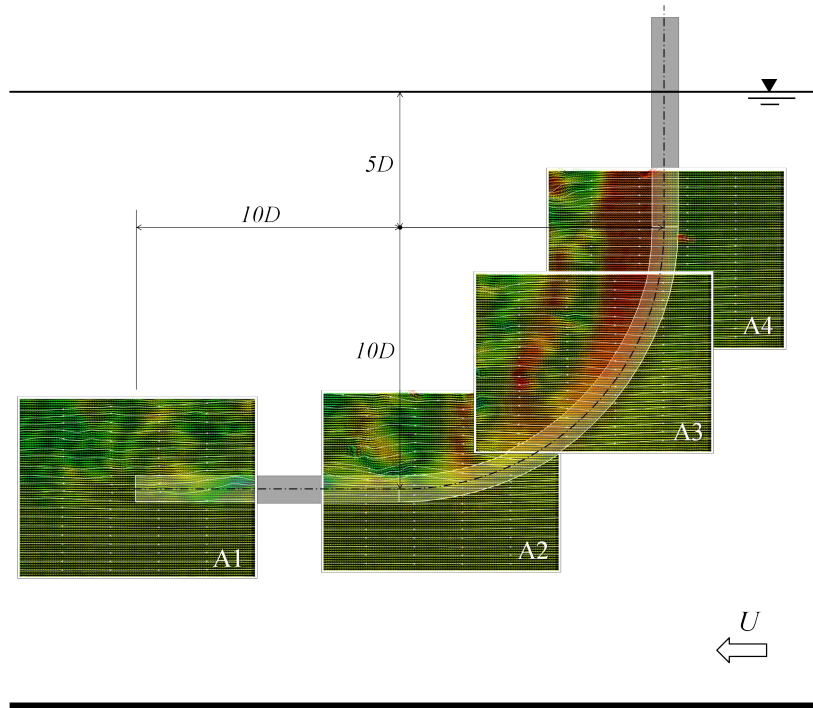


Figure 10: Composition of instantaneous PIV velocity fields for convex configuration with $h/D = 5$.

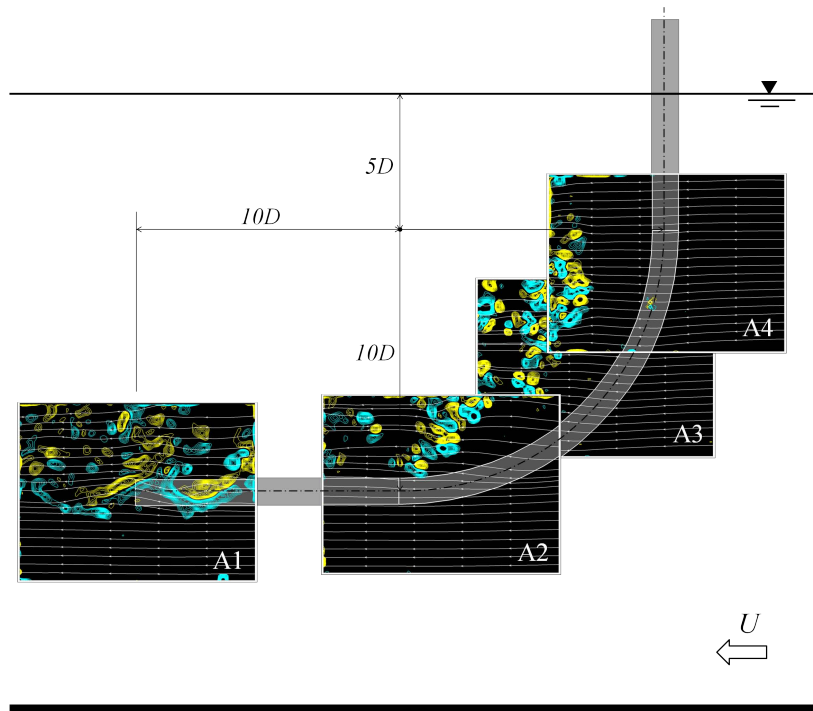


Figure 11: Composition of instantaneous PIV vorticity fields for convex configuration with $h/D = 5$.

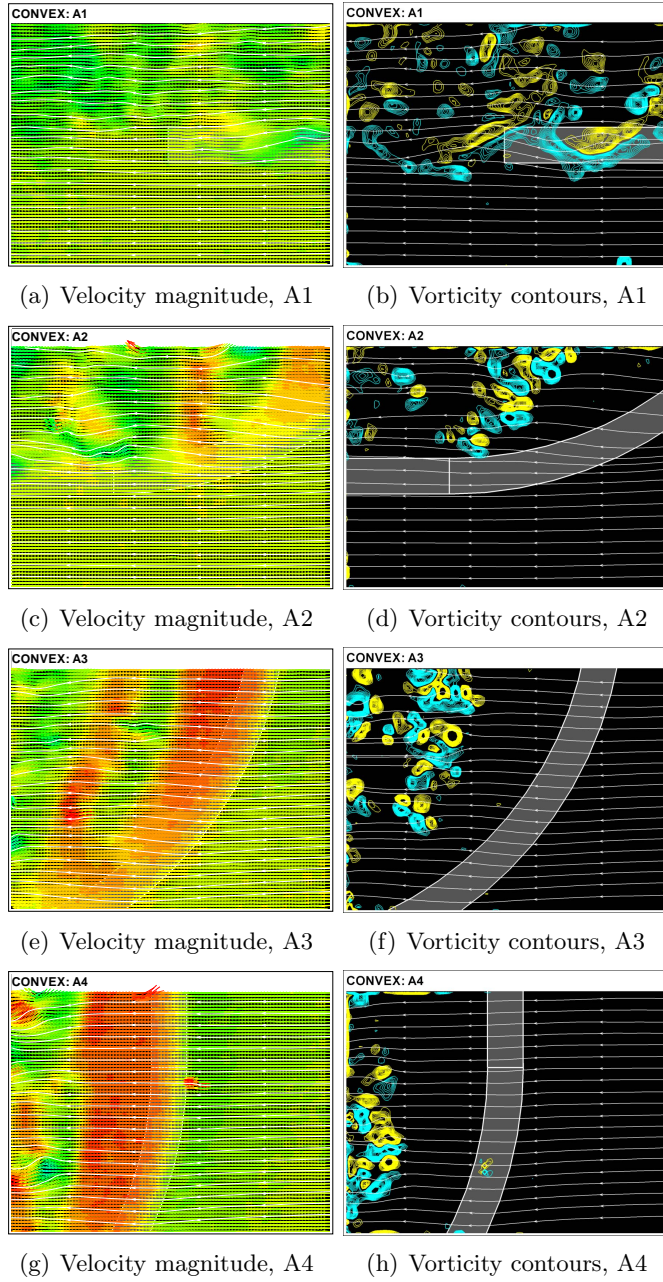


Figure 12: Detailed velocity and vorticity fields from Figures 10 and 11. Flow direction is from right to left. $Re = 1000$. Colour scale for velocity magnitude is from 0.004m/s (blue) to 0.05m/s (red). Colour scale for vorticity contours is in the range $\pm 0,004\text{s}^{-1}$. (Velocity fields do not correspond to the vorticity fields in time.)

335 Secondly, looking at the upper half of the body (A3 and A4) we notice
336 much stronger and coherent vortex tubes when compared to the flow around
337 the concave configuration. Area A3 reveals some kind of vortex dislocation
338 after a formation region that increases in length as we move upwards. Be-
339 cause the convex geometry does not encourage the vortex tubes to stretch
340 and break, a periodic wake seems to be sustained farther downstream. In
341 contrast with the flow around the concave configuration, the velocity field
342 around the curved section has a non-negligible vertical component upwards.
343 It is stronger in A2 and is gradually reduced as we move upwards along the
344 curvature in A3. This looks similar to Figure 3 in Miliou et al. (2007) for
345 $Re = 100$.

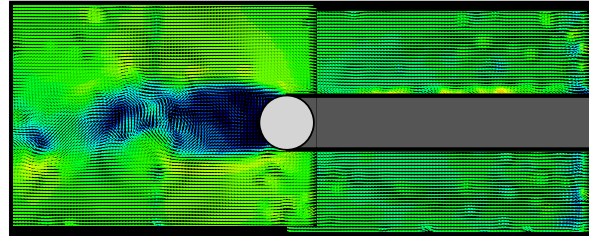
346 Gallardo et al. (2011) stated that there is a certain degree of alignment
347 of the flow structures with the axial curvature of the cylinder, which tilts
348 the flow structures with respect to the vertical direction. Figures 12(e) and
349 12(f) capture this behaviour, also recognised in Figure 2 of Gallardo et al.
350 (2011) and Figure 8 of Miliou et al. (2007).

351 5.2. Horizontal planes

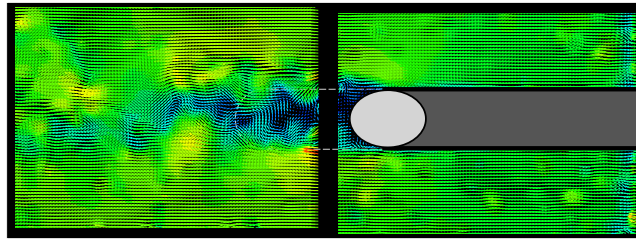
352 Figures 13 and 14 present PIV velocity fields for the three horizontal
353 planes indicated by H1, H2 and H3 in Figure 1. All measurements were
354 performed with $h/D = 5$. Plane H1 was positioned at the transition from
355 the straight to the curved section of the model, i.e., $5D$ below the water
356 line. Plane H2 was located $5D$ below that position and plane H3 another
357 $5D$ down towards the floor.

358 Figure 13 presents results for the concave configuration. The two cam-
359 eras were positioned underneath the model as viewing from the bottom
360 through the glass floor. A light grey circle or ellipse marks the cross section
361 of the cylinder at the illuminated plane. A dark grey rectangle represents
362 the part of the curved model in front of the laser plane, while a dashed line
363 illustrates the projection of the model behind the plane. Each image is com-
364 posed of two PIV areas taken simultaneously; for some cases they overlap,
365 for others they are apart.

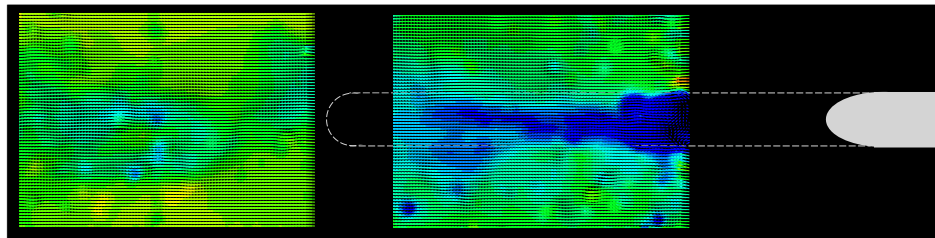
366 In Figure 13(a), for the horizontal plane at the transition from the
367 straight to the curved section, we notice a wider wake with a longer for-
368 mation region that generates stronger vortices. This formation is related
369 to the strong vortex tubes parallel to the straight section presented in Fig-
370 ure 9(g). Moving down to plane H2, the cross section of the cylinder turns
371 into an ellipse. The wake becomes much narrower with a short formation
372 length and no strong vortices are distinguishable in the downstream flow.
373 Figure 9(e) also showed that an oblique vortex tube would form closer to



(a) Plane H1

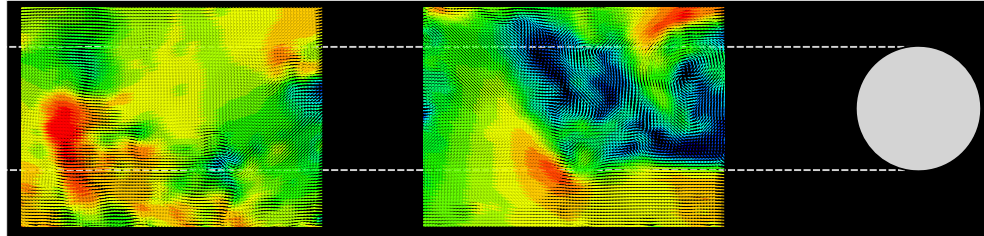


(b) Plane H2

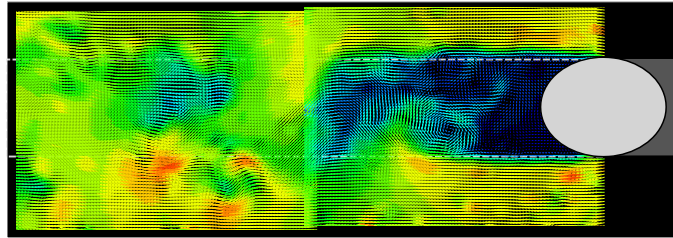


(c) Plane H3

Figure 13: Velocity fields for horizontal planes across the concave configuration. Please refer to Figure 1 for positions. Flow direction is from right to left. $Re = 1000$. Colour scale for velocity magnitude is from 0.004m/s (blue) to 0.05m/s (red).



(a) Plane H1



(b) Plane H2

Figure 14: Velocity fields for horizontal planes across the convex configuration. Please refer to Figure 1 for positions. Flow direction is from right to left. $Re = 1000$. Colour scale for velocity magnitude is from 0.004m/s (blue) to 0.05m/s (red).

374 the cylinder with vortices breaking apart into smaller eddies. Farther down
 375 to plane H3, the cross section illuminated by the laser plane now shows the
 376 beginning of the horizontal portion of the model. No vortex wake is iden-
 377 tified, but only a region of disturbed flow which agrees with pattern shown
 378 in Figure 9(c).

379 Results for the convex configuration in Figure 14 were obtained in the
 380 same way as the concave, the only difference being that the cameras were
 381 installed above the channel, viewing from the top through the free surface.
 382 As a consequence, plane H3 does not result in any useful velocity field once
 383 the flow that separates from the cylinder follows attached to the horizontal
 384 portion of the model, as seen in Figure 12(c).

385 Figure 14(a) presents velocity fields for the the first plane H1 at the
 386 transition region. A rather wide wake with strong vortical structures is
 387 noticeable through high induced velocities. Again, the same pattern was
 388 captured on the vertical PIV shown in Figure 12(g). Moving down to plane
 389 H2 we notice that an organised wake may still exist, even though the cross
 390 section of the cylinder turned into an ellipse. Vortex tubes were also ver-
 391 ified to persist further downstream in Figures 12(c) and 12(e) as coherent
 392 flow structures appeared periodically downstream of the cylinder in the flow

393 fields. Similar vortex structures were verified by Miliou et al. (2007) and
394 Gallardo et al. (2011). This proves that the convex configuration is more
395 prone to produce correlated vortex tubes along the curved length of the
396 cylinder, while in the concave configuration vortices soon break apart as
397 they are convected downstream.

398 Based on the results of Gallardo et al. (2011) for the convex configu-
399 ration, one can observe that the interaction of the shear layers and thus
400 the vortex formation length is a function of the cross-sectional shape being
401 circular or elliptical, here represented by different planes along the cylinder
402 span as can be seen in Figure 14 and also in Figure 3 of Gallardo et al.
403 (2011).

404 Plane H1 in Figure 14(a), which corresponds to plane $z/D = 16$ in
405 Gallardo et al. (2011), shows that the shear layers interact in a farther
406 downstream position from the body and the wake is wider compared to a
407 horizontal position of the H2 plane in Figure 14(b) where the cross-section of
408 the cylinder is elliptical. In the latter case, seen also at the $z/D = 8$ plane in
409 Gallardo et al. (2011), there are vortices produced within the recirculation
410 region exhibiting the wavier shear layers.

411 6. The excitation mechanism

412 The main question to be answered by the present study is concerned
413 with the fact that the amplitude in the cross-flow direction for the convex
414 configuration is able to drop down to 0.1 for high reduced velocities while
415 the concave configuration sustains vibration around 0.35. We believe this
416 distinct behaviour between the convex and the concave configurations is
417 related to the wake interference happening in the lower half of the cylinder
418 due to perturbations generated in the horizontal section when it is positioned
419 upstream.

420 In the concave configuration the horizontal part of the cylinder is located
421 upstream of the curved and vertical parts. The approaching flow encoun-
422 ters a circular blunt leading edge with a clear separation region around the
423 circumference (Figure 9(a)). The flow that separates at the leading edge
424 tends to create a separation bubble and latter reattaches along the horizon-
425 tal section of the cylinder. Because the cylinder already presents cross-flow
426 and streamwise vibrations, the three-dimensional separation bubble will not
427 find a stable configuration nor a definite reattachment region, instead it will
428 develop a periodic behaviour that may result in three-dimensional vortices
429 being shed downstream, reaching the other parts of the cylinder. This is
430 very clear in areas A1 and A2 of Figures 7 and 9 for the static cylinder.

431 The fluid-elastic mechanism behind the response may be a composition
432 of different phenomena acting at the same time. We believe this interac-
433 tion between the disturbed flow from the upstream horizontal part with the
434 curved and vertical parts is responsible for sustaining the level of vibration
435 around $\hat{y}/D = 0.35$ and $\hat{x}/D = 0.35$. We suggest such an interaction may
436 be occurring in the following forms:

437 (i) Vortices generated along the horizontal section may impinge on the
438 curved part generating impulses in the same manner that large eddies of
439 turbulence induce buffeting on elastic structures. Because the concave con-
440 figuration has a longer section immersed in such a disturbed wake it is more
441 susceptible to buffet. Evidence that a buffeting-like phenomenon might be
442 occurring is that the streamwise vibration shows a considerable increase
443 in amplitude with increasing flow speed further out of the synchronisation
444 range. Figure 6(b) also reveals that these vibrations are not harmonic and
445 may even be chaotic, another evidence supporting the buffeting-excitation
446 hypothesis.

447 (ii) The disturbed flow from the horizontal part may be disturbing and
448 disrupting the vortex shedding mechanism from the curved and vertical sec-
449 tions, for example uncorrelating the vortex shedding mechanism in a curved
450 region of the cylinder near the horizontal part. Also, the vortex wake along
451 the curved-vertical half of the concave cylinder showed less correlation along
452 the span, resulting in a lower peak of vibration during the synchronisation
453 range.

454 (iii) Because the concave configuration has a fixed separation ring at the
455 circle facing upstream, there might be some galloping-like instability related
456 to the separation and reattachment of the three-dimensional bubble. This
457 could generate non-resonant forces that could sustain some level of vibration
458 for reduced velocities above the synchronisation range.

459 (iv) Finally, the concave configuration might experience some kind of
460 instability related to the geometric arrangement of the experiment. Because
461 the centre of pressure is located upstream of the vertical axis of the pendulum
462 a minute deflection of the cylinder may result in a resolved force that will
463 increase displacement. The opposite is true for the convex configuration in
464 which the centre of pressure downstream of the vertical axis of the pendulum
465 can only generate stabilising forces.

466 Of course all four mechanisms suggested above may also be occurring
467 simultaneously or it may not even be possible to explain them separately.
468 In addition, they might as well be very dependent on Reynolds number and
469 amplitude of vibration.

470 **7. Conclusions**

471 We have experimentally investigated the two-degree-of-freedom VIV re-
472 sponse of a rigid, curved circular cylinder with a low mass-damping ratio.
473 With regard to the approaching flow (Reynolds number is in the range of
474 750-15,000) both concave and convex configurations were considered and the
475 measured responses were compared with those of a typical straight cylinder.
476 In summary, we conclude that:

477 (i) In general terms, a curved cylinder presents a lower peak of amplitude
478 of vibration in both the cross-flow and streamwise direction when compared
479 to a straight cylinder. Nevertheless, a considerable level of streamwise vi-
480 bration, not attributed to VIV, was observed for reduced velocity as high as
481 18.

482 (ii) Although the peak amplitude is reduced, a curved cylinder may
483 present a significant level of vibration that is sustained for higher values of
484 reduced velocity beyond the end of the typical synchronisation range.

485 (iii) The concave configuration shows a considerable level of cross-flow
486 vibration around $\hat{y}/d = 0.35$ up to the highest reduced velocity performed
487 in this experiment.

488 (iv) The overall response showed little dependency on the vertical length
489 immediately below the water line, at least for a section varying between
490 $h/D = 0$ and 10.

491 (v) From the PIV study on a stationary curved cylinder, we suggest
492 that the flow-structure interaction mechanism that differentiates the concave
493 from the convex cylinder response may have its origin in the disturbed flow
494 that separates from the horizontal part located upstream. This could be
495 related to buffeting, galloping, disturbed VIV or geometric instabilities.

496 Future work should concentrate on correlated PIV analyses of the vor-
497 tex formation along the curvature as well as on measurements of the flow
498 field on planes perpendicular to the plane of curvature. An investigation of
499 the interference effect generated by the separation at the tip of the horizon-
500 tal section could also help towards understanding the response. PIV and
501 instantaneous force measurements for an oscillating cylinder, especially at
502 high reduced velocities, could throw some light into the actual mechanism
503 of excitation.

504 **Acknowledgements**

505 G.R.S. Assi wishes to acknowledge the support of CNPq (308916/2012-
506 3) and FAPESP (11/00205-6). C.M. Freire acknowledges support from

507 FAPESP (10/00053-9). N. Srinil is grateful to the “Sir David Anderson
508 Award” from the University of Strathclyde and the “Early Career Researcher
509 International Exchange Award” supported by The Scottish Funding Council.
510 cil.

511 **References**

- 512 Assi, G.R.S., Meneghini, J.R., Aranha, J.A.P., Bearman, P.W., Casaprima,
513 E. **2006** Experimental investigation of flow-induced vibration interference
514 between two circular cylinders. *J. Fluids and Structures*, 22, 819-827.
- 515 Assi, G.R.S., Bearman, P.W and Kitney, N **2009** Low Drag Solutions for
516 Suppressing Vortex-Induced Vibration of Circular Cylinders. *J. Fluids and*
517 *Structures* 25, 1-10.
- 518 Assi, G.R.S., Bearman, P.W., Meneghini, J.R. **2010** On the wake-induced
519 vibration of tandem circular cylinders: the vortex interaction excitation
520 mechanism *J. Fluid Mech.*, 661, 365-401.
- 521 Assi, G.R.S., Bearman, P.W., Kitney, N., Tognarelli, M.A. **2010b** Suppres-
522 sion of Wake-Induced Vibration of Tandem Cylinders with Free-to-Rotate
523 Control Plates. *J. Fluids and Structures*, 26, 1045-1057.
- 524 Bearman, P.W. **1984** Vortex shedding from oscillating bluff bodies. *Annu.*
525 *Rev. Fluid Mech.*, 16, 195-222.
- 526 Freire, C.M., Korkischko, I., Meneghini, J.R. **2009** Development of an elastic
527 base with tow degrees of freedom for VIV studies. *In the proceedings of*
528 *COBEM 2009 – 20th International Congress of Mechanical Engineering*,
529 2009, Gramado, Brazil.
- 530 Freire, C.M., Meneghini, J.R. **2010**. Experimental investigation of VIV on a
531 circular cylinder mounted on an articulated elastic base with two degrees-
532 of-freedom. *In the proceedings of BBVIV6 – IUTAM Symposium on Bluff*
533 *Body Wakes and Vortex-Induced Vibrations*, 2010, Capri, Italy.
- 534 Freire, C.M., Korkischko, I., Meneghini, J.R. **2011** Definning a parame-
535 ter of effectiveness for the suppression of vortex-induced vibration. *In*
536 *the proceedings of OMAE2011 – 30th International Conference on Ocean,*
537 *Offshore and Arctic Engineering*, 2011, Rotterdam, The Netherlands.
- 538 Gallardo, J. P., Pettersen, B., Andersson, H. I. **2011** Dynamics in the tur-
539 bulent wake of a curved circular cylinder. *J. Phys. Conf. Ser.* 318, 062008.

- 540 Miliou, A., De Vecchi, A., Sherwin, S.J., Graham, M.R. **2007** Wake dynam-
541 ics of external flow past a curved circular cylinder with the free stream
542 aligned with the plane of curvature *J. Fluid Mech.*, 592, 89-115.
- 543 Srinil, N. **2010** Multi-mode interactions in vortex-induced vibrations of flex-
544 ible curved/straight structures with geometric nonlinearities *J. Fluids and*
545 *Structures*, 26, 1098-1122.
- 546 Williamson, C. H. K. **1996** Vortex dynamics in the cylinder wake *Annu.*
547 *Rev. Fluid Mech.*, 28, 477-539.